Available online at www.sciencedirect.com
ScienceDirect
Journal of Solid State Chemistry 179 (2006) 3541–3549
JOURNAL OF SOLID STATE CHEMISTRY
www.elsevier.com/locate/jssc

The new silver(I)thioantimonate(III) $[C_4N_2H_{14}][Ag_3Sb_3S_7]$ and a new structural variant of the silver(I)thioantimonate(III) $[C_2N_2H_9]_2[Ag_5Sb_3S_8]$ both synthesized under solvothermal conditions

V. Spetzler, C. Näther, W. Bensch*

Institut für Anorganische Chemie, Christian-Albrechts-Universität Kiel, Olshausenstr. 40, D-24098 Kiel, Germany

Received 20 April 2006; received in revised form 6 July 2006; accepted 18 July 2006
Available online 21 July 2006

Abstract

The novel silver(I)thioantimonates(III) $[C_4N_2H_{14}][Ag_3Sb_3S_7]$ (**I**) ($C_4N_2H_{12}$ = 1,4-diaminobutane) and $[C_2N_2H_9]_2[Ag_5Sb_3S_8]$ (**II**) ($C_2N_2H_8$ = ethylenediamine) were synthesized under solvothermal conditions using $AgNO_3$, Sb, S and the amines as structure directing molecules. Both compounds crystallize as orange needles with lattice parameters $a = 6.669(1)$ Å, $b = 30.440(3)$ Å, $c = 9.154(1)$ Å for I (space group *Pnma*), and $a = 6.2712(4)$ Å, $b = 15.901(1)$ Å, $c = 23.012(2)$ Å, $\beta = 95.37(1)^\circ$ for II (space group $P2_1/n$). In both compounds the primary building units are trigonal SbS_3 pyramids, AgS_3 triangles and AgS_4 tetrahedra. In **I** the layered $[Ag_3Sb_3S_7]^{2-}$ anion is constructed by two different chains. An $[Sb_2S_4]$ chain running along [100] is formed by vertex sharing of SbS_3 pyramids. The second chain contains a Ag_3SbS_5 group composed of the AgS_4 tetrahedron, two AgS_3 units and one SbS_3 pyramid. The Ag_3SbS_5 units are joined via S atoms to form the second chain which is also directed along [100]. The layered anion is then obtained by condensation of the two individual chains. The organic structure director is sandwiched by the inorganic layers and the shortest inter-layer distance is about 6.4 Å. In **II** the primary building units are linked into different six-membered rings which form a honeycomb-like layer. Two such layers are connected via Ag–S bonds of the AgS_4 tetrahedra giving the final undulated double layer anion. The structure directing ethylenediamine cations are located in pairs between the layers and a sandwich-like arrangement of alternating anionic layers and organic cations is observed. The inter-layer separation is about 5.4 Å. Both compounds decompose in a more or less complex manner when heated in an argon atmosphere. The optical band gaps of about 1.9 eV for the two compounds proof the semiconducting behavior. For **II** the conductivity was measured with impedance spectroscopy and amounts to $\sigma_{295K} = 7.6 \times 10^{-7}\,\Omega^{-1}\,cm^{-1}$. At 80 °C the conductivity is significantly larger by one order of magnitude.

Keywords: Thioantimonates; Solvothermal synthesis; Crystal structures; Thermoanalytical measurements; Optical properties; Impedance spectroscopy

1. Introduction

During the last few years the number of thioantimonates(III) containing a transition metal ion (TM^{n+}) as a part of the SbS_x network increased steadily [1–17]. One of the first groups of such compounds were the series of isostructural thioantimonates(III) $Mn_2Sb_2S_5 \cdot L$ (L = methyleamine, ethylamine, 1,3-diaminopropane, diethylenetriamine, *N*-methyl-1,3-diaminopropane) and copper-thioantimonates(III) $[L]Cu_2SbS_3$ (L = ethylendiamine, 1,3-DAP = 1,3-diaminopropane, 1,4-Dab = 1,4-diaminobutane, 1,6-diaminohexane, 1,4-di-(2-aminoethyl)-piperazine, diethylenetriamine) [8,13,14]. Another series of Cu(I)thioantimonates(III) with composition $[L]Cu_3Sb_2S_5$ (L = diethylenetriamine triethylenetetramine) were reported very recently [14]. In all the Cu compounds protonated amines act as structure directors and they are arranged in the galleries between the anionic layers. Hence, these compounds may be regarded as inorganic/organic composite materials. There are some examples with silver like the minerals Miargyrite $AgSbS_2$ [18], Pyrargyrite Ag_3SbS_3 [19], and Stephanite Ag_5SbS_4 [20]. Silver is incorporated into anionic frameworks in $RbAg_2SbS_4$, Rb_2AgSbS_4, KAg_2SbS_4,

*Corresponding author. Fax: +49 4341 880 1520.
E-mail address: wbensch@ac.uni-kiel.de (W. Bensch).

0022-4596/$ - see front matter © 2006 Elsevier Inc. All rights reserved.
doi:10.1016/j.jssc.2006.07.022

K_2AgSbS_4 [21], $[C_2H_9N_2]_2[Ag_2SbS_3]$, $[C_2H_9N_2]_2[Ag_5Sb_3S_8]$ [22] and $[C_6H_{20}N_4][Ag_5Sb_3S_8]$ [23]. In many of these inorganic/organic hybrid compounds the anionic part is layered with the amines being sandwiched by the anions. In the present contribution the crystal structures, thermal stability and optical spectroscopy data for the compounds $[C_4N_2H_{14}][Ag_3Sb_3S_7]$ (**I**) and $[C_2N_2H_9]_2[Ag_5Sb_3S_8]$ (**II**) are presented. In addition, we present results of the impedance spectroscopy of compound **II**.

2. Experimental details

2.1. Syntheses

The two compounds $[C_4N_2H_{14}][Ag_3Sb_3S_7]$ (**I**) and $[C_2N_2H_9]_2[Ag_5Sb_3S_8]$ (**II**) were prepared under solvothermal conditions in Teflon-lined steel autoclaves. For **I** a mixture of $AgNO_3$ (2 mmol), Sb (2 mmol), S (5 mmol) and 4 mL 1,4-diaminobutane was heated at 140 °C for 7 days. Compound **II** was synthesized applying a mixture of $AgNO_3$ (2 mmol), Sb (2 mmol), S (4 mmol) and 4 mL ethylenediamine. The slurry was heated at 140 °C for 5 days followed by cooling to room temperature. The products were collected by filtration and washed with deionized water, acetone and dried in vacuum. Both compounds crystallized as orange needles. The yield was about 80% for **I** and 60% for **II** based on Ag. In both cases red needles of $AgSbS_2$ were present as the second phase. The compounds are stable on air. Analytical data from CHNS-Analysis: found for I: C: 4.9%, H: 1.3%, N: 2.9%; Calcd.: C: 4.8%, H: 1.2%, N: 2.8%, found for II: C: 2.3%, H: 0.9%, N. 2.4%; Calcd.: C: 2.1%, H: 0.7%, N: 2.3%.

3. X-ray scattering studies

The X-ray intensity data were collected at 293 K using a STOE IPDS-1 using MoK_α radiation ($\lambda = 0.71073$ Å). The raw intensities were treated in the normal way applying a Lorentz, polarization correction. The data were also corrected for absorption effects. The structures were solved using SHELXS-97 [24]. Crystal structure refinements were done against F^2 with SHELXL-97 [25]. All non-hydrogen atoms were refined with anisotropic displacement parameters. The hydrogen atoms were positioned with idealized geometry and refined with fixed isotropic displacement parameters using a riding model.

After the refinement of the structure of I a large electron density maximum of 7.86 e/Å^3 was located 1.36 Å from Ag(2). According to the distances to neighbored S atoms it can be assumed that Ag(2) is disordered over at least two different positions. In contrast to Ag(2), the split position Ag(2′) has no bond to S(4) but is displaced slightly in the direction of Sb(2). In the early stages of the refinement the site occupation factors of both split positions were refined and were then fixed at 80:20 ratio. Regardless of this procedure the anisotropic displacement parameters for Ag(2) and Ag(2′) were large, and the ellipsoids are elongated especially in the direction of the Ag(2)–Sb(2) vector. Therefore, some mobility of Ag(2) cannot be excluded. In the next refinement steps further split positions were used for Ag(2) and Ag(2′). But the structure model was not significantly improved, strong correlations between the variables were observed and the anisotropic displacement parameters were still elongated in the direction of Sb(2). At this stage the two position model with Ag(2)/Ag(2′) was selected as the model to describe the structure. Details of data collections and refinement results are summarized in Table 1. Bond lengths and angles are listed in Tables 2, 3, and 4.

Table 1
Selected crystallographic data and refinement results for $[C_4N_2H_{14}][Ag_3Sb_3S_7]$ (**I**) and $[C_2N_2H_9]_2[Ag_5Sb_3S_8]$ (**II**)

	I	**II**
a (Å)	6.669(1)	6.2712(4)
b (Å)	30.440(3)	15.901(1)
c (Å)	9.154(1)	23.012(2)
β/°	*95.37(1)*	
V/A^3	1858.2(3)	2290.7(3)
d_{calc}/g cm^{-3}	3.587	3.715
crystal system	Orthorhombic	Monoclinic
space group	*Pnma*	$P2_1/n$
2θ/deg	4–56	4–56
hkl range	$-7 \leqslant h \leqslant 7$	$-8 \leqslant h \leqslant 8$
$-35 \leqslant k \leqslant 36$	$-21 \leqslant k \leqslant 21$	
$-10 \leqslant k \leqslant 10$	$-30 \leqslant k \leqslant 30$	
No. coll refl	13349	22614
No. unique refl.	1648	5303
refl $F_o > 4\sigma(F_o)$	1536	4202
Params	98	215
R1 $(F_o > 4\sigma(F_o))$	0.0346	0.0332
wR2 $(F_o > 4\sigma(F_o))$	0.0888	0.0768
R1 (all refl)	0.0371	0.0471
wR2 (all refl)	0.0909	0.0815
GOF	1.082	1.025
δ(F)/e Å^{-3}	−2.272/2.245	−2.78/3.55

3.1. Raman spectroscopy

The Raman spectra were measured from 100 to 3500 cm^{-1} with a Bruker IFS 66 Fourier transform Raman spectrometer (wavelength: 514.5 nm, $T = 20$ K).

3.2. Thermoanalytical investigations

Thermogravimetric analyses were performed using a Netzsch STA 429 DTA-TG device. The samples were heated in Al_2O_3 crucibles at a rate of 4 K min^{-1} to 400 °C under a flow of argon of 100 ml min^{-1}.

3.3. Impedance spectroscopy

The measurements were done with the so-called Kieler cell in an argon atmosphere using a HP 4192 Impedance-Analizer at 5 Hz–13 MHz with gold electrodes. The

Table 2
Selected interatomic distances (Å) and angles (°) for $[C_4N_2H_{14}][Ag_3Sb_3S_7]$ (**I**). Estimated standard deviations are given in parentheses.

Sb(1)–S(1)	2.4050(16)	Ag(1)–Ag(1)[c]	3.3349(4)
Sb(1)–S(2)[a]	2.4616(15)	Ag(1)–Ag(2)	3.2874(14)
Sb(1)–S(2)	2.4859(15)	Ag(2)–S(4)[e]	2.390(3)
Sb(2)–S(4)	2.421(3)	Ag(2)–S(3)[b]	2.647(2)
Sb(2)–S(3)	2.4240(16)	Ag(2)–S(3)	2.647(2)
Sb(2)–S(3)[b]	2.4240(17)	Ag(2)–S(4)[c]	2.944(4)
Ag(1)–S(1)	2.4658(17)	Ag(2)–Ag(1)[c]	3.1821(13)
Ag(1)–S(3)	2.5322(17)		
Ag(1)–S(4)[c]	2.5484(14)		
S(1)–Sb(1)–S(2)[a]	96.69(5)	S(2)[a] –Sb(1)–S(2)	84.82(4)
S(4)–Sb(2)–S(3)	94.39(6)	S(3)–Sb(2)–S(3)[b]	101.60(9)
S(1)–Ag(1)–S(3)	131.01(6)	S(1)–Ag(1)–S(4)[c]	121.50(7)
S(3)–Ag(1)–S(4)[c]	107.01(7)	S(4)[e] –Ag(2)–S(3)	133.73(4)
S(3)[b] –Ag(2)–S(3)	90.43(8)	S(4)[e] –Ag(2)–S(4)[c]	95.80(9)
S(3)[b] –Ag(2)–S(4)[c]	93.71(6)		

Symmetry codes:
[a] i + 0.5,*y*,−z + 0.5; [b] *x*,−*y* + 1.5; *z*; [c] *x*−0.5,*y*,−*z* + 1.5; [d] *x* + 0.5,*y*,−*z* + 1.5; [e] *x*−1,*y*,*z*.

Table 3
Intermolecular N···S distances (Å) in $[C_4N_2H_{14}][Ag_3Sb_3S_7]$ (**I**) and $[C_2N_2H_9]_2[Ag_5Sb_3S_8]$ (**II**)

	II	**I**
N···S	2.536 (S8)	2.403 (S2)
	2.556 (S7)	2.561 (S1)
	2.827 (S2)	2.599 (S1)
	2.790 (S7)	2.876 (S2)
	3.004 (S2)	2.994 (S1)

Table 4
Selected interatomic distances (Å) and angles (°) for $[C_2N_2H_9]_2[Ag_5Sb_3S_8]$ (**II**)

Sb(1)–S(1)	2.4241(18)	Ag(3)–S(2)[f]	2.8132(18)
Sb(1)–S(2)	2.5100(15)	Ag(3)–S(4)^{2x}	2.5440(16)
Sb(1)–S(3)	2.4085(15)	Ag(3)–S(6)	2.6993(17)
Sb(2)–S(2)[a]	2.5243(15)	Ag(4)–S(3)	2.5546(16)
Sb(2)–S(4)^{2x}	2.4290(17)	Ag(4)–S(4)^{2x}	2.6678(17)
Sb(2)–S(5)	2.3887(15)	Ag(4)–S(6)	2.6785(16)
Sb(3)–S(6)	2.4348(17)	Ag(4)–S(7)[b]	2.6621(17)
Sb(3)–S(7)	2.4127(15)	Ag(5)–S(1)[a]	2.6032(19)
Sb(3)–S(8)	2.4184(15)	Ag(5)–S(5)[a]	2.5122(17)
Sb(1)–Ag(2)	3.1559(7)	Ag(5)–S(6)	2.6719(16)
Sb(2)–Ag(1)	3.0293(7)	Ag(5)–S(8)	2.976(2)
Ag(1)–S(1)	2.6376(16)	Ag(1)–Ag(4)[e]	3.2499(10)
Ag(1)–S(3)[b]	2.5407(17)	Ag(3)–Ag(4)	3.3659(9)
Ag(1)–S(7)[b]	2.5007(16)	Ag(3)–Ag(5)	3.0708(9)
Ag(2)–S(5)[e]	2.5903(18)	Ag(2)–S(4)	2.5349(16)
Ag(3)–S(1)[a]	2.5512(16)	Ag(2)–S(8)[d]	2.4968(17)
S(1)–Sb(1)–S(2)	100.52(6)	S(4)–Ag(4)–S(6)	99.70(5)
S(3)–Sb(1)–S(1)	98.65(6)	S(3)–Ag(4)–S(7)[b]	104.72(5)
S(3)–Sb(1)–S(2)	91.11(5)	S(7)[b] –Ag(4)–S(4)	113.79(5)
S(5)–Sb(2)–S(2)[a]	90.32(5)	S(3)–Ag(4)–S(4)	114.92(5)
S(5)–Sb(2)–S(4)	101.16(6)	S(3)–Ag(4)–S(6)	126.58(6)
S(4)–Sb(2)–S(2)	103.10(5)	S(5)[a] –Ag(5)–S(6)	118.57(6)
S(7)–Sb(3)–S(8)	100.61(5)	S(5)[a] –Ag(5)–S(1)[a]	123.18(5)
S(8)–Sb(3)–S(6)	101.55(6)	S(1)[a] –Ag(5)–S(6)	108.21(5)
S(7)–Sb(3)–S(6)	100.51(5)	S(7)[b] –Ag(1)–S(1)	126.32(6)
S(3)[b] –Ag(1)–S(1)	96.23(5)	S(7)[b] –Ag(1)–S(3)[b]	119.46(5)
S(8)[c] –Ag(2)–S(4)	134.66(6)	S(8)[c] –Ag(2)–S(5)[d]	114.69(6)
S(4) –Ag(2)–S(5)[d]	101.83(5)	S(4)–Ag(3)–S(1)[a]	126.49(6)
S(4)–Ag(3)–S(6)	102.37(5)	S(4)–Ag(3)–S(2)[e]	106.01(5)
S(6)–Ag(3)–S(2) [e]	110.34(5)		

Symmetry codes: [a] −*x* + 1.5, *y* + 0.5, −*z* + 1.5; [b] *x* + 1, *y*, *z*; [c] *x* + 0.5, *y*−0.5, −*z* + 1.5; [d] *x*−1, *y*, *z*; [e] −*x* + 0.5, *y* + 0.5, −*z* + 1.5; [f] −*x* + 1.5, *y*−0.5, −*z* + 1.5.
Estimated standard deviations are given in parentheses.

temperature was controlled with a Cr/CrNi thermocouple. Non-blocking interfaces/electrodes behave like a resistance (R) and capacitance (C) in parallel. This leads to a semicircle in the so-called Nyquistplot which has a high frequency limit at the origin and a low-frequency limit at $Z' = R$. At the maximum of the semicircle the capacitance can be evaluated. Additionally, the interface impedance has a Warburg impedance W in series with R [26–28]. For compound **II** a non-blocking effect was observed with the slow diffusion of the species (Ag^+) crossing the interface indicated by a Nyquist-diagram with the Warburg impedance. The Warburg impedance (W) arises from the fact that the concentration of a species at an electrode surface is out of phase by 45° with the flux of the same species across the surface [26–28].

4. Results and discussion

The new compound $[C_4N_2H_{14}][Ag_3Sb_3S_7]$ (**I**) crystallizes in the orthorhombic space group *Pnma* with four formula units in the unit cell (Table 1). The atoms Sb(2), Ag(2) and S(4) are located on special positions whereas all other unique atoms are on general positions. The two Ag atoms are surrounded by 3 S atoms to form AgS_3 triangles with Ag–S bonds ranging from 2.390(3) to 2.647(2) Å. The corresponding S–Ag–S angles are between 90.43(8) and 133.73(4)°. The geometrical parameters are comparable to those observed in $AgSbS_2$ [18], Ag_3SbS_3 [19], Ag_5SbS_4 [20], or $[C_2N_2H_9]_2[Ag_5Sb_3S_8]$ [22]. Ag(2) has another contact to a S atom at the long distance of 2.944(4) Å, i.e. the polyhedron around Ag(2) is a strongly distorted tetrahedron (Fig. 1, Table 2).

The Ag(1) atom is situated 0.0991 Å above the plane formed by the three S atoms. The Ag–Ag separations (Table 2) are significantly longer than in metallic Ag. The Sb–S bond lengths and S–Sb–S angles in the two unique trigonal SbS_3 pyramids are in the typical range observed for this environment (Table 2) [1–17]. The two-dimensional $[Ag_3Sb_3S_7]^{2-}$ anion is constructed by condensation of two different chains. The Sb(1)S_3 units form an one-dimensional $[Sb_2S_4]$ chain by vertex sharing running along [100] (Fig. 2, top). Another chain is formed by interconnection of the Ag(1)S_3, Ag(2)S_4 and Sb(2)S_3 moieties. The AgS_4 unit shares two edges with two AgS_3 triangles and one edge with SbS_3 yielding an Ag_3SbS_5 group with a distorted

Ag_3SbS_3 semi-cube as central motif (Fig. 2, bottom). The Ag_3SbS_5 units are joined by three S(4) atoms to form a chain directed along [100].

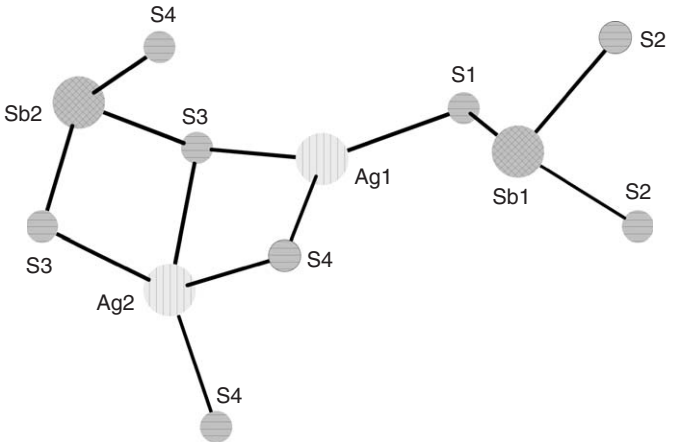

Fig. 1. The primary building units in compound **I** together with labeling. Note that the disordered Ag2′ atom is not displayed.

This central chain is bridged by the $^{1}{}_{\infty}[Sb_2S_4]$ chain forming the final layered $[Ag_3Sb_3S_7]^{2-}$ anion extending in the (010) plane (Fig. 3). An interesting structural detail is the unusual bind mode of S(4) which has bonds to 4 Ag and 1 Sb atoms (see Fig. 2, bottom).

In contrast to compound **II** where no so-called secondary Sb–S bonds are found, the Sb(1) atom in **I** has two such contacts at 3.399 and 3.423 Å. The amine cations are located in pairs between the layers and the two NH_3 groups of the amines are oriented toward the networks forming a sandwich-like arrangement with an interlayer distance of 7.4 Å (Fig. 3, top). The short intermolecular N–H···S distances with H···S separations ranging from 2.403 to 2.994 Å indicate hydrogen bonding interactions between the anionic layers and the structure directing ammonium ions (Table 3).

The compound $[C_2N_2H_9]_2[Ag_5Sb_3S_8]$ (**II**) crystallizes in the monoclinic space group $P2_1/n$ with four formula units in the unit cell (Table 1). Five crystallographically independent Ag atoms, three Sb and eight S atoms are found in **II**. Two trigonal AgS_3 units (Ag(1), Ag(2)), three AgS_4 tetrahedra (Ag(3), Ag(4), Ag(5)) and three trigonal

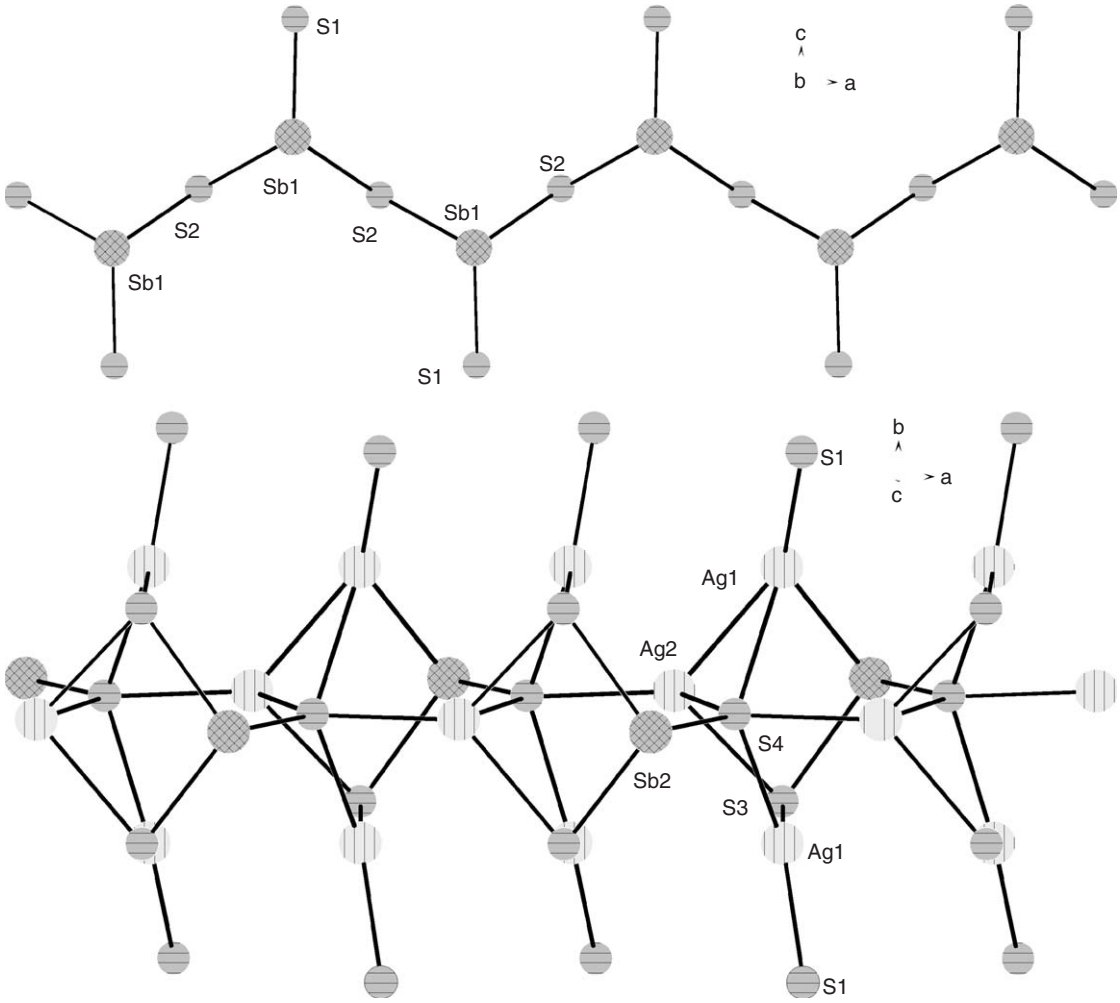

Fig. 2. The one-dimensional $[Sb_2S_5]$ chain in **I** formed by interconnection of the $Sb(1)S_3$ pyramids (top) and the Ag_3SbS_5 units joined by the S(4) atoms (bottom).

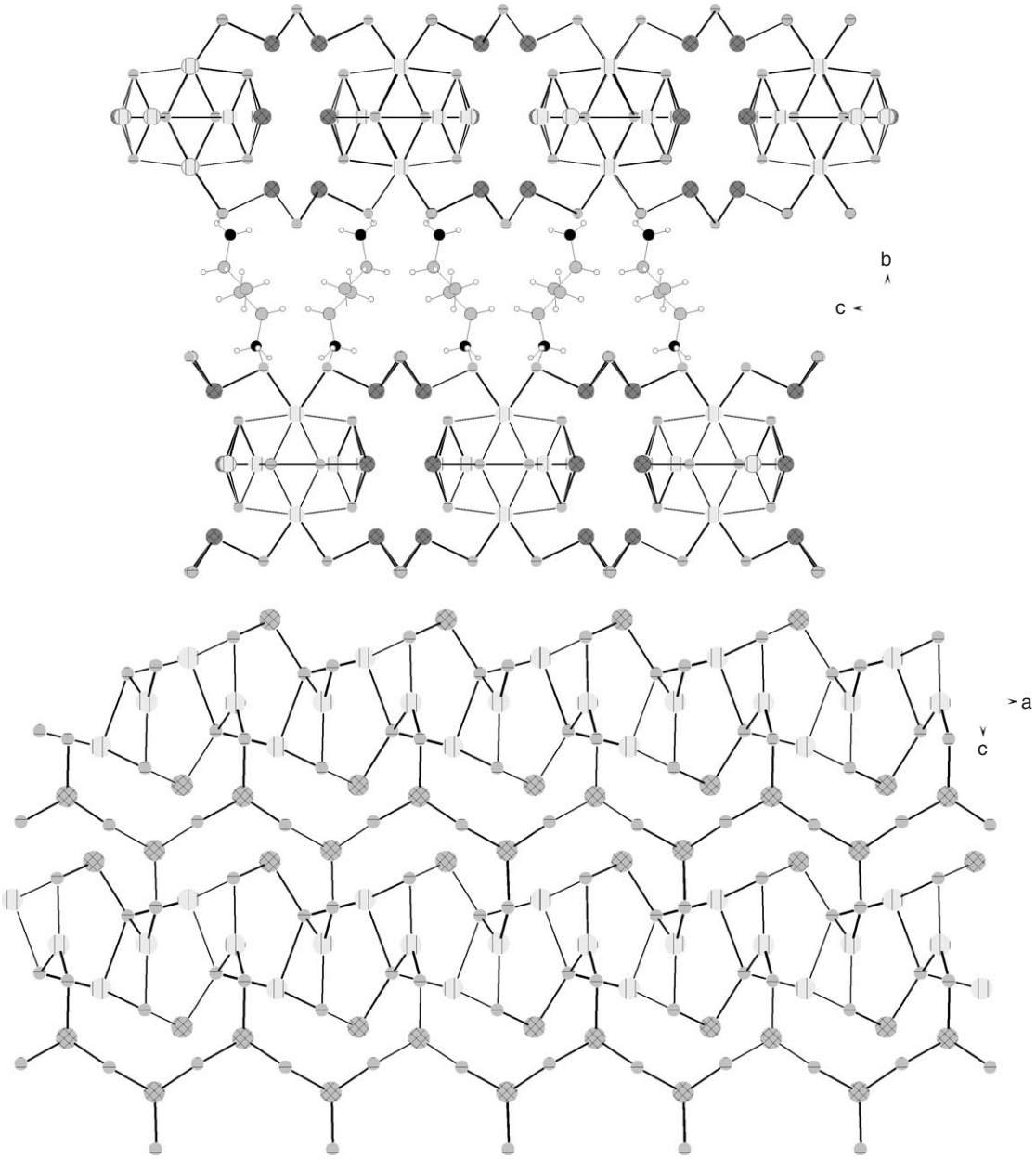

Fig. 3. Two different views of the layers in **I**. Top: View along [100] showing the sandwich-like arrangement of the anionic layers and the organic cations. Bottom: View along [010] showing the interconnection of the two different chains.

SbS_3 pyramids are the primary building units (PBUs) (Fig. 4). The Ag–S distances in the AgS_3 groups are between 2.497(2) and 2.638(2) Å with S–Ag–S angles ranging from 96.23(5)° to 134.66(6)° (Table 4). The Ag–S bonds are longer than in minerals like Miargyrite $AgSbS_2$ (Ag–S: 2.36 to 2.58 Å) [18] or Pyrargyrite Ag_3SbS_3 (Ag–S average: 2.40 Å) [19], but they match well with data for Stephanite Ag_5SbS_4 [20], MAg_2SbS_4, and M_2AgSbS_4 (M = K, Rb) [21], $[C_2N_2H_9]_2[Ag_5Sb_3S_8]$ [22] or $[C_6H_{20}N_4]$ $[Ag_5Sb_3S_8]$ [23]. The Ag atoms are situated 0.6224 Å (Ag(1)) and 0.4259 Å (Ag(2)) above the planes formed by the three S atoms. Ag(1) has Sb(2) at a distance of 3.0293(7) Å as next nearest neighbor. Assuming that the electron lone pair of Sb(2) is located opposite to the plane of the three S atoms in the $Sb(2)S_3$ pyramid it points towards the Ag(1) atom, similar to what was observed in copper-thioantimonates [13,14]. The $Ag(3,4,5)S_4$ tetrahedra are severely distorted with Ag-S bonds from 2.512(2) Å to 2.976(2) Å and corresponding angles between 89.23(5)° and 126.58(6)°. The Sb-S bond lengths (Table 4) are typical for the well known trigonal pyramidal SbS_3 unit [1–17]. The Ag(3) and Ag(5) atoms are 3.071(1) Å apart, which is longer than in Ag metal (2.89 Å), while Ag–Ag distances in Ag_5SbS_4 [20] and $[C_2H_9N_2]_2[Ag_2SbS_3]$ [22] are with 2.91 Å shorter than in **II**, suggesting weak d^{10}–d^{10} interactions which are significant for Ag–Ag distances < 3.3 Å [29]. The next-nearest S atoms of Sb are at distances larger than the sum of the van der Waals radii of 3.80 Å.

The first layer shows a honeycomb-like arrangement of eight different condensed six-membered rings: Ag(1,4)Sb(3)S_3, Ag(1,4)Sb(1)S_3, Ag(1,3)Sb(1)S_3, Ag(3)Sb(1,2)S_3, Ag(2,3)Sb(2)S_3, Ag(2,5)Sb(2)S_3, Ag(2,5)Sb(3)S_3, and Ag(4,5)Sb(3)S_3 (Fig. 5). Seven of these rings are composed of two Ag, one Sb and three S atoms and the eighth ring contains one Ag, two Sb and three S atoms (Fig. 5). The layer is connected to a symmetry related layer via Ag(3,4,5)–S bonds to form a buckled double layer extending in the (001) plane, and due to the 2_1 screw axis and the *n* glide plane the different rings are located above and/or below each other (see Fig. 6).

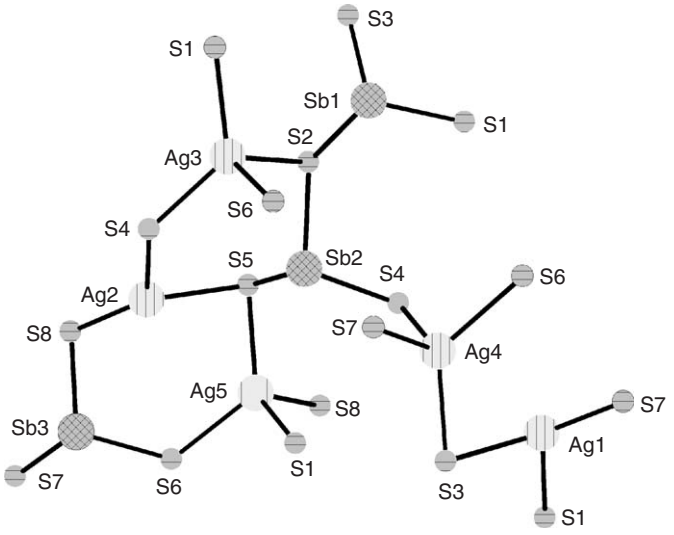

Fig. 4. The primary building units in compound **II** together with atom labeling.

The cations are located in pairs between the layers and a sandwich-like arrangement is observed (Fig. 6), similar to what was previously observed in other thioantimonate-s(III) [13,14]. Relatively short H···S distances ranging from 2.536 to 3.004 Å indicate hydrogen bonding interactions (Table 3). The shortest interlayer distance amounts to 5.4 Å.

We note that two compounds with the $[Ag_5Sb_3S_8]^{2-}$ anion were reported recently. Both compounds were prepared under solvothermal conditions in the presence of ethylenediamine as structure director [22,23], and the first is denoted as **III**. This compound crystallizes in space group *Pm* and the layered anion is constructed by interconnection of four SbS_3 pyramids, three AgS_4 tetrahedra, two AgS_3 triangles and one bend AgS_2 group. The Ag atom of this latter unit has a S atom at a large distance of about 3.17 Å. Like in **II** honeycomb-like sheets are produced by fused six-membered rings (seven Ag_2SbS_3 and one $AgSb_2S_3$ rings), and buckled double layers are formed. A remarkable difference between the two compounds are the short Ag–Sb separations of 2.868 and 2.985 Å in **III** compared to the shortest distances of 3.029 and 3.156 Å in **II**. The arrangement of the cations is also different in the two compounds. In **III** the *en* molecules occur in pairs with short N···N separations of 2.40–2.63 Å whereas the shortest N···N distances in **II** are 2.828 and 2.778 Å. Furthermore, the interlayer distance is about 0.6 Å larger in **III** than in **II**. The other thioantimonate(III) with the

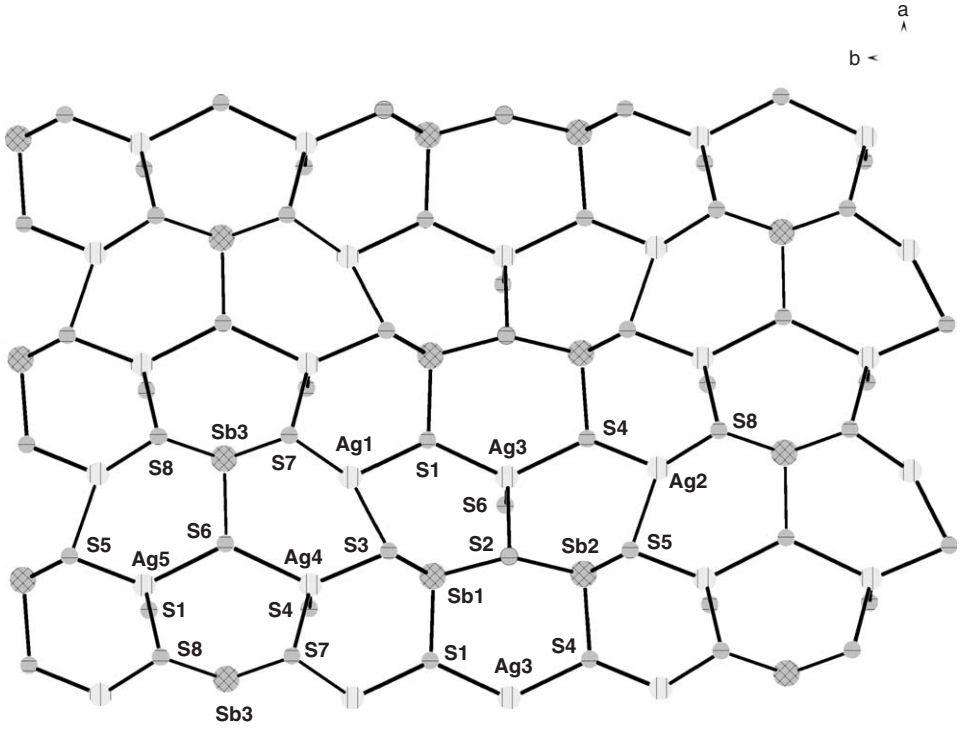

Fig. 5. The condensed six-membered rings in compound **II** forming a single layer.

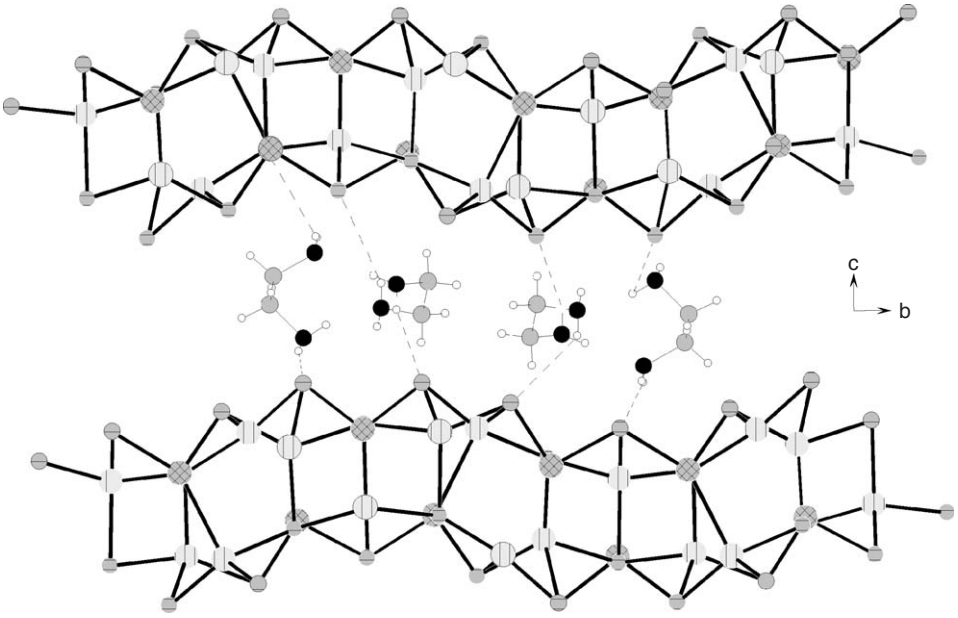

Fig. 6. The buckled double layers in compound **II** with view along [100] and the arrangement of the organic cations. Dotted lines indicate S···H hydrogen bonding.

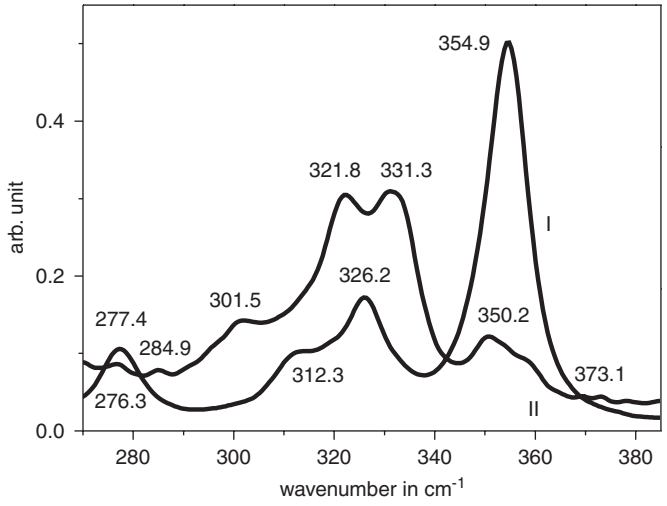

Fig. 7. Raman spectra of $[C_4N_2H_{14}][Ag_3Sb_3S_7]$ (**I**) and $[C_2N_2H_9]_2[Ag_5Sb_3S_8]$ (**II**).

$[Ag_5Sb_3S_8]^{2-}$ ion was prepared with triethylenetetramine (TETN) as structure director [23], and is denoted as **IV**. The compound crystallizes in $P2_1/m$ with two SbS_3 units, two AgS_4 tetrahedra and one AgS_3 moiety. Again, six-membered rings are formed by vertex linking of these building units to form honeycomb-like double layers. The bond lengths in the AgS_3 groups and AgS_4 tetrahedra are in a narrower range than in **II**. The TETN molecule adopts a C-shaped geometry and the shortest interlayer separation is about 6.3 Å. All three compounds crystallize in monoclinic space groups with very similar *a*- and *b*-axes, but very different values for the *c*-axis and the monoclinic angle β.

4.1. Optical spectroscopy

Charge compensation requires that the amine molecules are monoprotonated in **I** and diprotonated in **II**. In the IR spectra the absorptions located at 1100, 1400, 1600, 2400 and 3400 cm^{-1} are typical for R–NH_3^+ groups, evidencing the presence of protonated amine groups. In the Raman spectra (Fig. 7) the most intense resonances are located at 354.9 cm^{-1}, 326.2 cm^{-1} and 277.4 cm^{-1} for **I** and at 331.3 cm^{-1} and 321.8 cm^{-1} for **II**. Weak bands are observed at 312.3 cm^{-1} for **I** and at 276.3 cm^{-1}, 284.9 cm^{-1}, 301.5 cm^{-1}, 350.2 cm^{-1} and 373.1 cm^{-1} for **II**. The bands between 362 cm^{-1} and 339 cm^{-1} are typical for SbS_3 units [31,32]. The optical band gaps of both compounds were determined from transformed UV–Vis diffuse reflectance spectra in the usual way (Kubelka–Munk). The optical band gaps of about 1.9 eV indicate that the compounds are semiconductors. These values are similar to values obtained for copper thioantimonates [13,14,30].

4.2. Impedance spectroscopy

Impedance spectroscopy was performed using a pressed pellet of **II**. From the Nyquist plot (Fig. 8) the resistance at room temperature was estimated as $R_{RT} = 4.2 \times 10^5\,\Omega$, the conductivity $\sigma_{RT} = 7.6 \times 10^{-7}\,\Omega^{-1}\,cm^{-1}$ and the capacitance $C_{RT} = 0.1$ nF. With increasing temperature the resistance decreases reaching $5.3 \times 10^4\,\Omega$ at 80 °C. The activation energy $E_A = 0.7$ eV was estimated applying the Arrhenius equation, but for Ag ion conductivity one would expect a lower value.

The difference between the optical band gap ($E_g =$ 1.9 eV) and the activation energy E_A (0.7 eV) can be explained by impurities or point defects in the material

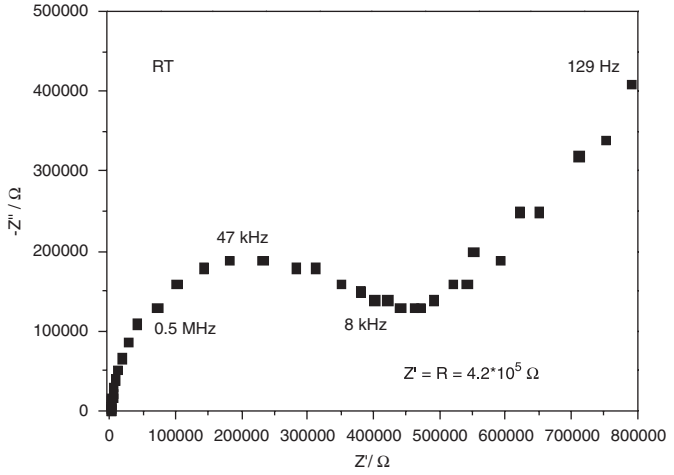

Fig. 8. Nyquist plot of the impedance measurement of a non-blocking interface at room temperature (**II**).

[26–28]. The impurities lead to an impurity level below the conduction band (donor level) and an impurity level above the valence band (acceptor level). At lower temperatures such impurities dominate the conductivity and at higher temperatures the intrinsic conduction mainly contributes to the electrical conductivity. In the present case the temperature regime covers the range where the intrinsic properties are measured. It is not unusual that the activation energy E_A differs from the optical band gap.

4.3. Thermal investigation

The DTA–TG–DTG curves are shown in Fig. 9. Compound **I** starts to decompose at $T_{onset} = 196\,^{\circ}C$ with a strong endothermic signal at $T_p = 213\,^{\circ}C$. The total weight loss of 12.1% is in good agreement with the calculated value ($-\Delta m_{theo} = 12.4\%$). In the dark gray residue only minute amounts of CHN are present. The second endothermic event at $T_p = 384\,^{\circ}C$ is not accompanied by a mass change and therefore, might correspond to the melting point of the decomposition product. In the X-ray powder pattern of the residue $AgSbS_2$ could be identified. Compound **II** seems to be less stable than **I** and decomposes in one step ($T_{onset} = 147\,^{\circ}C$) which is accompanied by an endothermic signal with a peak temperature $T_p = 169\,^{\circ}C$ and a weight loss of 8.9%. The expected value for the emission of two ethylenediamine molecules is 9.6%. A small thermal event occurs at $T_p = 376\,^{\circ}C$ which is not accompanied by a mass change and might be due to melting of an intermediately formed compound. The C, H, N elemental analysis of the gray residue yields a very low level of 0.56% for CHN. In the decomposition product the reflections of Ag_3SbS_3 and $AgSbS_2$ are identified in the X-ray powder pattern.

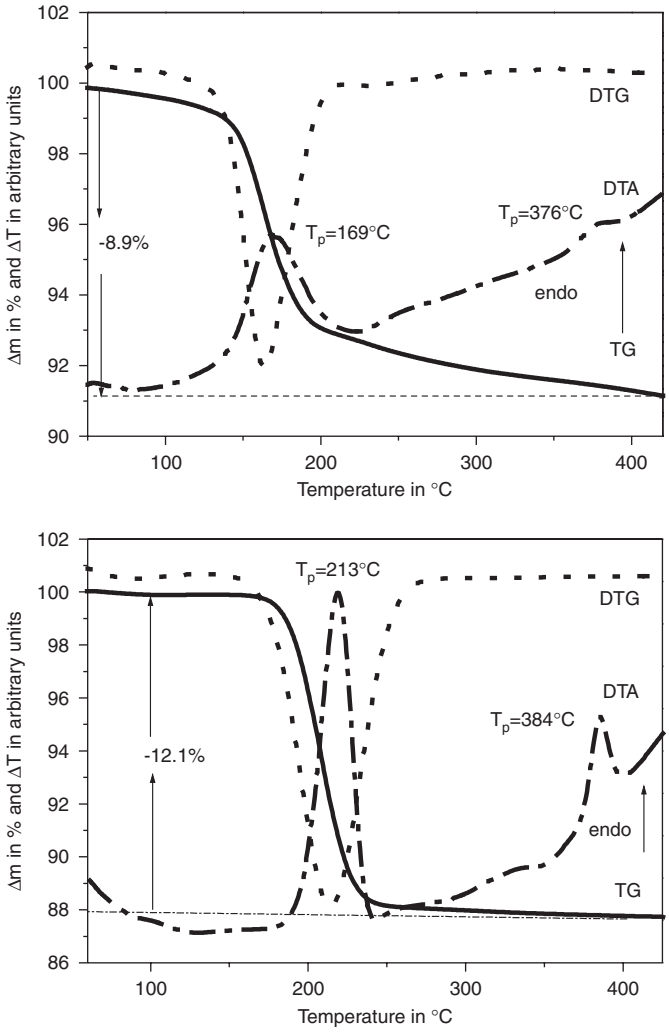

Fig. 9. TG–DTG–DTA curves of $[C_4N_2H_{14}][Ag_3Sb_3S_7]$ (**I**) (bottom) and $[C_2N_2H_9]_2[Ag_5Sb_3S_8]$ (**II**) (top).

5. Summary

Compared to the relatively large number of copper (I)thioantimonates(III) obtained under solvothermal conditions using organic cations as structure directors the number of silver(I)thioantimonates(III) is relatively low. In the two compounds **I** and **II** layers are formed by the interconnection of trigonal SbS_3 pyramids, AgS_4 tetrahedra and AgS_3 units. The network topologies are quite different reflecting the flexibility to adopt the requirements of the organic structure directing molecules. The protonated amines are sandwiched by the anionic layers and the compounds may be regarded as inorganic–organic hybrids with interlayer separations of 7.4 Å (**I**) and 5.4 Å (**II**). A larger range for such layer separations was observed for copper(I)thioantimonates(III) with values ranging from 4.43 to 8.44 Å [14]. For many host lattices like TaS_2 or vermiculites the interlayer expansion is independent from the number of C atoms for alkyl chains with less than 6 C atoms [33]. The same observation is made for the layered coin metal thioantimonate compounds. In all these compounds the ammonium groups of the organic molecules are oriented towards the anionic layers ensuring optimal S···H bonding interactions. Another interesting

aspect of the Ag thioantimonate chemistry is the occurrence of three topologically very similar $[Ag_5Sb_3S_8]^{2-}$ anions which were synthesized under different conditions. The differences of the syntheses of the two materials containing the *en* cation are different antimony sources, different Sb:Ag:S ratios and different temperatures. The previously reported compound [22] was obtained with a molar composition $Sb_2S_3 : AgNO_3 : S = 1:1:2.5$ (Sb : Ag : S = 2:1:5.5) at 190 °C whereas the title compound crystallized from a mixture with molar ratio Sb : $AgNO_3$: S = 1:1:2 at 140 °C. The observation that the two compounds are obtained under very different conditions may suggest that in solution the same building units exist.

References

[1] H.-O. Stephan, M.G. Kanatzidis, Inorg. Chem. 36 (1997) 6050–6057.
[2] W. Bensch, M. Schur, Z. Naturforsch. 52b (1997) 405–409.
[3] R. Kiebach, C. Näther, W. Bensch, Z. Anorg. Allg. Chem. 628 (2002) 2176–2181.
[4] R. Stähler, W. Bensch, Eur. J. Inorg. Chem. (2001) 3073–3078.
[5] R. Stähler, C. Näther, W. Bensch, Acta Crystallogr. C 57 (2001) 26–27.
[6] R. Stähler, W. Bensch, Z. Anorg. Allg. Chem. 628 (2002) 1657–1662.
[7] M. Schaefer, C. Näther, W. Bensch, Solid State Sci. 5 (2003) 1135–1139.
[8] L. Engelke, R. Stähler, M. Schur, C. Näther, W. Bensch, R. Pöttgen, M.H. Möller, Z. Naturforsch. 59b (2004) 869–876.
[9] M. Schaefer, R. Stähler, R. Kiebach, C. Näther, W. Bensch, Z. Anorg. Allg. Chem. 630 (2004) 1816–1822.
[10] A.V. Powell, S. Boissiere, A.M. Chippendale, J. Chem. Soc., Dalton Trans. (2000) 4192–4195.
[11] Zh. Chen, R.E. Dillks, R.-J. Wang, J.Y. Lu, J. Li, Chem. Mater. 10 (1998) 3184–3188.
[12] A.V. Powell, R. Paniagua, P. Vaqueiro, A.M. Chippindale, Chem. Mater. 14 (2002) 1220–1224.
[13] V. Spetzler, H. Rijnberk, C. Näther, W. Bensch, Z. Anorg. Allg. Chem. 630 (2004) 142–148.
[14] V. Spetzler, C. Näther, W. Bensch, Inorg. Chem. 44 (2005) 5805–5812.
[15] W. Bensch, M. Schur, Eur. J. Solid State Inorg. Chem. 33 (1996) 1149–1160.
[16] M. Schur, C. Näther, W. Bensch, Z. Naturforsch. 56b (2001) 79–84.
[17] R. Stähler, W. Bensch, J. Chem. Soc., Dalton Trans. (2001) 2518–2522.
[18] C.R. Knowles, Acta Crystallogr. 17 (1964) 847–851.
[19] D. Harker, J. Chem. Phys. 4 (1936) 381–390.
[20] B. Ribar, W. Nowacki, Acta Crystallogr. B 26 (1970) 201–207.
[21] G.L. Schimek, W.T. Pennington, P.T. Wood, J.W. Kolis, J. Solid State Chem. 123 (1996) 277–284.
[22] P. Vaqueiro, A.M. Chippindale, A.R. Cowley, A.V. Powell, Inorg. Chem. 42 (2003) 7846–7851.
[23] A.V. Powell, J. Thun, A.M. Chippindale, J. Solid State Chem. 178 (2005) 3414–3419.
[24] G.M. Sheldrick, SHELXS-97, Program for Crystal Structure Determination, University of Göttingen, Germany, 1997.
[25] G.M. Sheldrick, SHELXL-97, Program for the Refinement of Crystal Structures, University of Göttingen, Germany, 1997.
[26] R.D. Armstrong, T. Dickensen, P.M. Willis, Electroan. Chem. Interf. Electrochem. 53 (1974) 389–397.
[27] F. Sauerwald, Dissertation, Geowissenschaften der Philipps-Universität Marburg 2005.
[28] C.J. Wen, C. Ho, B.A. Boukamp, I.D. Raistrick, W. Weppner, R.A. Huggens, Inter. Met. Rev. 5 (1981) 253–259.
[29] M. Jansen, Angew. Chem. 99 (1987) 1136–1149.
[30] V. Spetzler, R. Kiebach, C. Näther, W. Bensch, Z. Anorg. Allg. Chem. 630 (2004) 2398–2404.
[31] A. Pfitzner, Chem. Eur. J. 3 (1997) 2032–2038.
[32] A. Pfitzner, D. Kurowski, Z. Kristallogr. 215 (2000) 373–376.
[33] A. Lerf, in: H.S. Nalwa (Ed.), Handbook of Nanostructured Materials and Nanotechnology, Vol. 5, Academic Press, New York, 2000.